$CsPbBr_3$ QD/AlO_x inorganic nanocomposites with exceptional stability in water, light and heat

A. Loiudice,[+[a]] S. Saris,[+[a]] E. Oveisi,[[b]] D. T. L. Alexander,[[b]] and R. Buonsanti*[[a]]

Abstract: Herein, the assembly of $CsPbBr_3$ QD/AlO_x inorganic nanocomposite, using atomic layer deposition (ALD) for the growth of the amorphous alumina matrix (AlOx), is proven as a novel protection scheme for this new class of QDs. The nucleation and growth process of AlOx on the QD surface was thoroughly investigated by a miscellanea of techniques which highlighed the importance of the interaction between the ALD precursor and the QD surface to uniformely coat the QDs while preserving the optoelectronic properties. These nanocomposites show an exceptional stability against exposure to air (for at least 45 days), irradiation under simulated solar spectrum (for at least 8h), to thermal treatment (at least up to 200ºC in air), and finally against immersion in water. The method was extended to assembly $CsPbBr_xI_{3-x}$ QD/AlO_x and $CsPbI_3$ QD/AlO_x nanocomposites which were more stable compared to the pristine QD films.

In the last year, all-inorganic perovskite quantum dots ($CsPbX_3$ QDs with X = Br, I, Cl) have emerged as a new class of semiconductor nanocrystals with outstanding optical properties and with huge promise in QD-based photovoltaics, light emitting diodes and lasing applications.[1–5] One of the main issues that still remains is to achieve stability against air, temperature, light irradiation and water. In addition to their implementation in optoelectronic devices, developing strategies to stabilize the perovskite QDs is crucial to explore their intrinsic optoelectronic properties, which may require relatively long measurements in air and under light.[6,7] Currently, a few attempts have been made to stabilize $CsPbX_3$ QDs.[8-15] As one example, Pan et al. have demonstrated stability in air at high optical fluence for more than one day by passivating their surface with didodecyl dimethylammonium sulphide.[8] The introduction of poly(maleicanhydride-alt-1-octadecene) during the synthesis of $CsPbX_3$ QDs has been suggested to improve their stability during irradiation under UV light.[9] At the same time this treatment was not enough to prevent structural degradation, as sintering and phase transition were still observed. Palazon et al. have discovered increased stability in air and water upon exposure of $CsPbX_3$ QD films to a low flux of X-rays for 5 hours as a result of the formation of intramolecular C=C bonding between adjacent ligands.[10] While this represents an interesting study, the as-obtained films were not uniformly stabilized and loss of luminescence in the central region and at the edges of the films was evident. Recently, Li et al. have utilized trimethylaluminum cross-linking on the surface of thin film perovskite QDs with the only purpose to prevent their dissolution in organic solvents. [11] Silica has also been used as a matrix to protect the inorganic perovskite QDs.[12,13] While increased stability in solution was demonstrated with this approach, long-term stability in thin films has not been studied. The bottom line is that, while for organic-inorganic perovskites different stabilizing approaches have been successfully implemented, based mostly on polymers, no reliable approach exists for inorganic perovskite QDs.[14],[15]

Herein, the encapsulation with an amorphous alumina (AlO_x) matrix deposited by atomic layer deposition (ALD) is proposed as an effective strategy to stabilize $CsPbX_3$ QDs. Compared to the protection schemes mentioned above, the advantages of the metal oxide encapsulation by ALD include conformity, uniformity and low solid-state ion diffusion coefficients.[16–19] Previous works have proven metal oxide matrices (Al_2O_3 and ZnO) to improve the oxidative and photothermal stability of other QDs (PbSe, PbS, CdSe, CdSe@ZnS and CdTe).[16–18,20–25] However, no application to the perovskite QDs has been reported so far. The high sensitivity to moisture, temperature and light of this class of QDs makes the development of an optimal ALD process not trivial. For example, low temperature and short water pulses, are mandatory to avoid QD degradation. In this work, a low temperature ALD process for the deposition of AlO_x on a $CsPbX_3$ QD thin film has been successfully developed. The AlO_x matrix protects the perovskite QDs from oxygen and moisture in air, confers them stability in water and prevents sintering, thus improving their stability at high temperature and under light exposure for hours. The process is of general applicability and has been successfully exploited for different composition, specifically for $CsPbBr_3$, $CsPbI_3$ and $CsPbBr_{3-x}I_x$.

[a] Dr. A. Loiudice, S. Saris
Department of Chemical Sciences and Engineering, EPFL Valais Wallis, CH-1951 Sion, Switzerland.
[b] Dr. E. Oveisi, Dr. D. T. L. Alexander
Interdisciplinary Centre for Electron Microscopy (CIME), EPFL, CH-1015 Lausanne, Switzerland.
[a] Prof. Buonsanti*
Department of Chemical Sciences and Engineering, EPFL Valais Wallis, CH-1951 Sion, Switzerland.
e-mail: raffaella.buonsanti@epfl.ch
+ A.L. and S.S. contributed equally to this work.

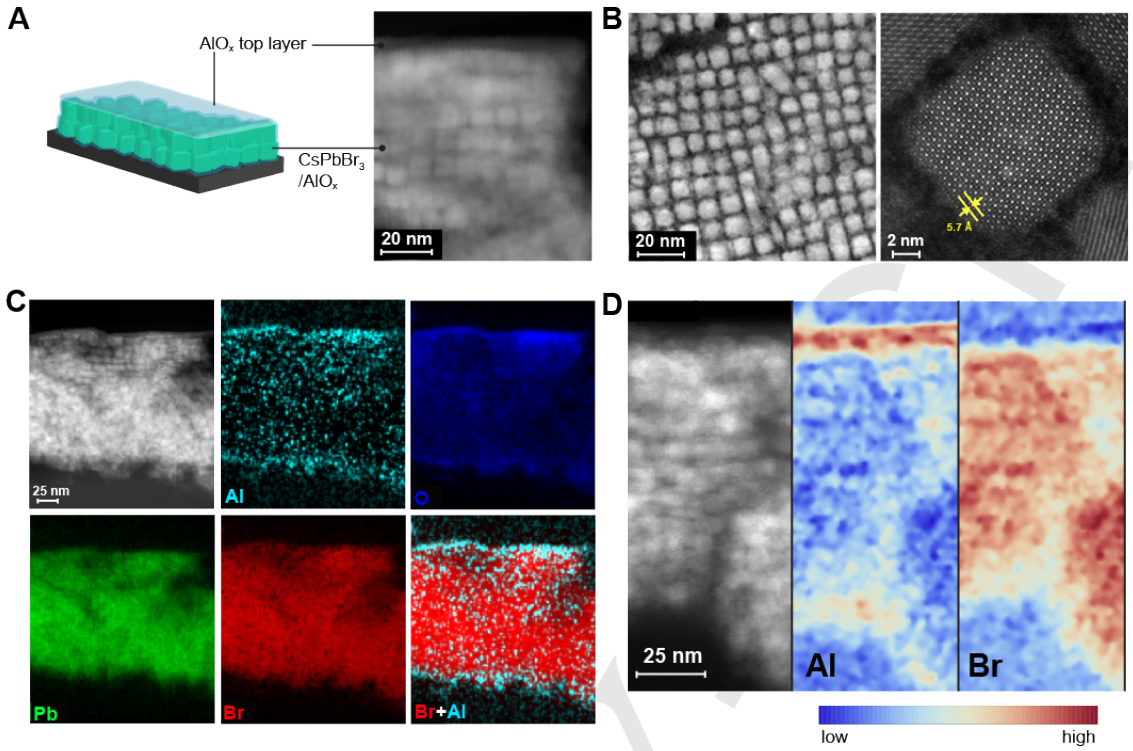

Figure 1. A) Schematic representation of the $CsPbBr_3/AlO_x$ nanocomposite and cross-sectional STEM-HAADF image of a typical nanocomposite obtained by performing 100 ALD alumina cycles on a 60nm thick QD film . B) In-plane STEM-HAADF image of $CsPbBr_3$ QD film infilled with AlO_x. C) Cross-sectional STEM-HAADF image and corresponding EDX elemental colored maps of Al, O, Pb, Br and Br+Al and D) EELS color-coded elemental intensity maps of Al and Br.

The $CsPbBr_3$ QDs, synthesized according to the procedure by Protesescu et al., were spin-coated on silicon or glass substrates before the ALD process (Figure S1).[1] The latter was carried at 50 ºC with trimethylaluminum (TMA) and H_2O as the precursor and the co-reactant, respectively. Low temperature was essential to avoid sintering and structural changes of the QDs (Figure S2).[26] Each deposition cycle consisted of TMA pulse (t1), purging (t2), H_2O pulse (t3), purging (t4). The ALD parameters were varied to identify the optimal conditions for a uniform protective coating without degrading the QDs. Optimal times were found to be t1 = 0.015 s, t2 = 10 s, t3 = 0.010 s and t4 = 180 s. Figure 1 gives an overview of the structural analysis conducted by different electron microscopy techniques to fully characterize a typical $CsPbBr_3$ QD/AlO_x inorganic nanocomposite film. Figure 1A shows a cross-sectional scanning transmission electron microscopy high angle annular dark field (STEM-HAADF) image of the $CsPbBr_3$ QD/AlO_x nanocomposite along with a sketch of the final structure. This analysis beautifully reveals that the QDs are embedded in the alumina matrix without any change of size and shape compared with the pristine QDs (Figure S1). In this sample an AlO_x overcoating layer of around 10 nm was measured in the STEM-HAADF image (Figure 1A). High resolution STEM-HAADF was also performed on single QDs covered with 5 cycles of AlO_x (Figure 1B). The alumina coating conferred stability to the QDs under the electron beam, and enabled high resolution imaging without special low dose techniques.[27] No change in the lattice parameters (5.7 Å) was observed compared with the reported values for $CsPbBr_3$ QDs.[28] The XRD patterns of the QD film before and after the AlO_x deposition were also identical (Figure S3). STEM-HAADF imaging and area selective energy-dispersive X-ray spectroscopy (EDX) maps are shown in Figure 1C. The Cs:Pb:Br ratio was constant at 1:1:3 in the EDX spectrum, indicating that the stoichiometry is preserved in the nanocomposites (Figure S4, Table 1). The higher Al atomic percentage on the top layer suggests that an alumina overcoating layer ultimately seals the QD film. To confirm the infilling of AlO_x in the interstices between the $CsPbBr_3$ QDs, STEM electron energy-loss spectroscopy (EELS) , which allows to distinguish the Al K edge from that of the Br L edge, was applied (Figure 1D) . In this way, the two signals, which overlap in EDX, could be mapped, confirming not only the pure Al-containing overcoating layer, but also identifying the ALD-deposited AlO_x bottom substrate layer. Finally, the infilling of the alumina throughout the $CsPbBr_3$ QD films and the absence of any noticeable change in chemical composition and oxidation states in the $CsPbBr_3$ QDs after the ALD process was corroborated by X-ray spectroscopy (XPS) (Figures S5 and S6). The XPS data gave also some insights into the stoichiometry of the amorphous alumina matrix, which is indicated as AlO_x because of the variable composition throughout the nanocomposite with a 2:3 stoichiometric ratio in the overcoat layer and a deviation from stoichiometry with increasing oxygen content in the infilling layer (Figure S6).

The nucleation and the growth steps of the alumina deposition process were studied by combining a miscellanea of techniques, including Fourier Transform Infrared Spectroscopy (FTIR), Nuclear Magnetic Resonance (NMR) Spectroscopy, Inductively Coupled Plasma Mass Spectrometry (ICP-MS), Scanning Electron Microscopy (SEM) and XPS.

Firstly, to elucidate the nucleation mechanism of the alumina on the surface of the QDs, XPS, NMR and FTIR were utilized (Figure 2). The nucleation of alumina in the ALD process requires the presence of polar groups on the solid surface, commonly hydroxyl groups (-OH).[25] Figure 2A shows representative XPS spectra corresponding to the Pb 4f core levels for the pristine QDs (black), the QDs after one TMA pulse (blue) and the final QD/AlO_x nanocomposite (red). In the peak deconvolution, the component at 137.6 eV in the pristine QDs and in the QD film after one TMA pulse corresponds to oxygen bonded lead (Pb-O), in agreement with O1s core level energy in Figure S5 indicating the presence of an oxygen-metal bond. The metallic lead may form under the XPS beam.[29] Typical FTIR spectra corresponding to the pristine QDs, the QDs after one TMA pulse and the final QD/AlO_x nanocomposite are reported in Figure 2B. The spectrum of the pristine QDs is consistent with the presence of long-chain aliphatic ligands (oleylamine and oleic acid).[30] After the TMA pulse, the main change in the spectrum is the appearance of two strong and sharp peaks at 1591 cm^{-1} and 1496 cm^{-1}, which are characteristic of the COO^- stretching modes. The FTIR spectrum corresponding to the nanocomposites shows a strong -OH peak centered around 3450 cm^{-1}. Such a signal is expected for an alumina grown by an ALD process at low temperature, which should contain many hydroxyl impurities.[18,31] The persistence of the carboxylate peaks in the nanocomposites indicates that the ligands do not decompose during the ALD process, which is reasonable considering the low temperature. The N1s and C1s signals present in the XPS depth profiling throughout the film thickness are in agreement with the FTIR (Figure S7). ^{1}H NMR spectra were recorded on QDs reacted with different amount of TMA. To make these experiments possible, a solution-based process was developed to mimic the reaction of the TMA with the QD surface during the ALD (see SI for experimental details). The alkene and the TMA spectral regions are included in Figure 3C and the full spectra are reported in Figure S8. The alkene resonances around 5.6 ppm correspond to the oleyl species, deriving from oleylamine and oleic acid, which are the native ligands for the $CsPbBr_3$ QDs.[30] As the TMA/NC ratio increases, changes in the alkene region indicate modification of the ligand shell while the broad and shifted resonance (compared to the pure compound, Figure S8) around -0.4 ppm strongly suggest that the TMA binds the NC surface.[30,32,33] Based on the XPS, FTIR and NMR data analysis, the following nucleation mechanism is speculated and sketched in Figure 2D. In the initial stage of nucleation, the TMA reacts with the partially oxidized NC surface, which is possible considering the degree of permeability to small molecules possessed by the ligand shell, and no change in the pristine ligand shell is observed in the NMR spectra (here the amount of TMA coordinating the surface is too low to be detected by NMR).[34],[35] Upon saturation of the oxidized surface sites, the TMA molecule intercalates at the hydrophilic ligand/QD interface as recently suggested by Li et al.[11]

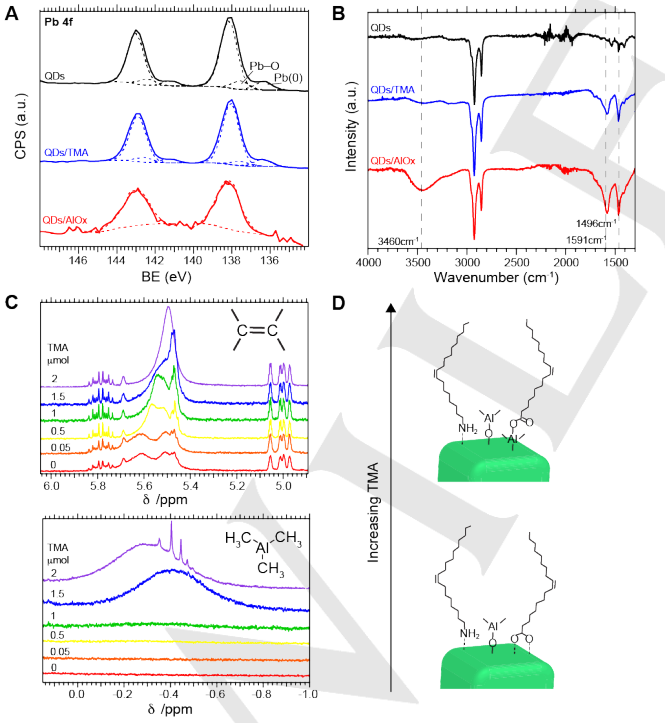

Figure 2. A) Pb 4f XPS spectra and B) FTIR spectra and of the pristine QD film (black), the QDs after one pulse of TMA (blue) and the final QD/AlO_x nanocomposite (red); C) ^{1}H NMR in the region of the alkene protons (top) and TMA protons (bottom) while varying the concentration of TMA. D) Scheme of the possible nucleation mechanism of alumina on the QD surface during the ALD process.

Secondly, to estimate the alumina growth per cycle (GPC), ICP-MS analysis was used as the main tool to calculate the amount of alumina deposited per each ALD cycle and complementary techniques supported the obtained trends (Figures S9 and S10). Two different growth regime were identified: Step 1 (number of cycles <75, GPC =1.06 ng cm^{-2} $cycle^{-1}$) and Step 2 (number of cycles >75, GPC = 0.21 ng cm^{-2} $cycle^{-1}$), which are associated with the infilling and the overcoating processes, respectively. The SEM cross-section analysis on QD films with different thickness and the same number of ALD cycles (Figure S10) reveals a consistent full infilling of the QD films up to a thickness of around 250 nm, when the pore clogging effect during ALD becomes evident.[36]

The comparison between the optical properties of the pristine QDs and the nanocomposites was then carried out (Figure S11). No significant change of the absorption features and no peak shift were observed, consistent with the absence of compositional and morphological changes from TEM, SEM, XRD and XPS analyses. However, a photoluminescence (PL) intensity decrease of around 50% with respect to the initial value was recorded (Figure S11). Such a change was too big to be solely attributed to the change of total reflectance due to the alumina matrix.[23] Several experiments were carried out to isolate the effects of different parameters on the PL decrease and are described in the Supporting Information. While the effects of temperature, time, reactants are interrelated and difficult to disentangle, the interaction of the TMA with the NC surface was determined to be the key factor in the PL quenching (Figure S12).

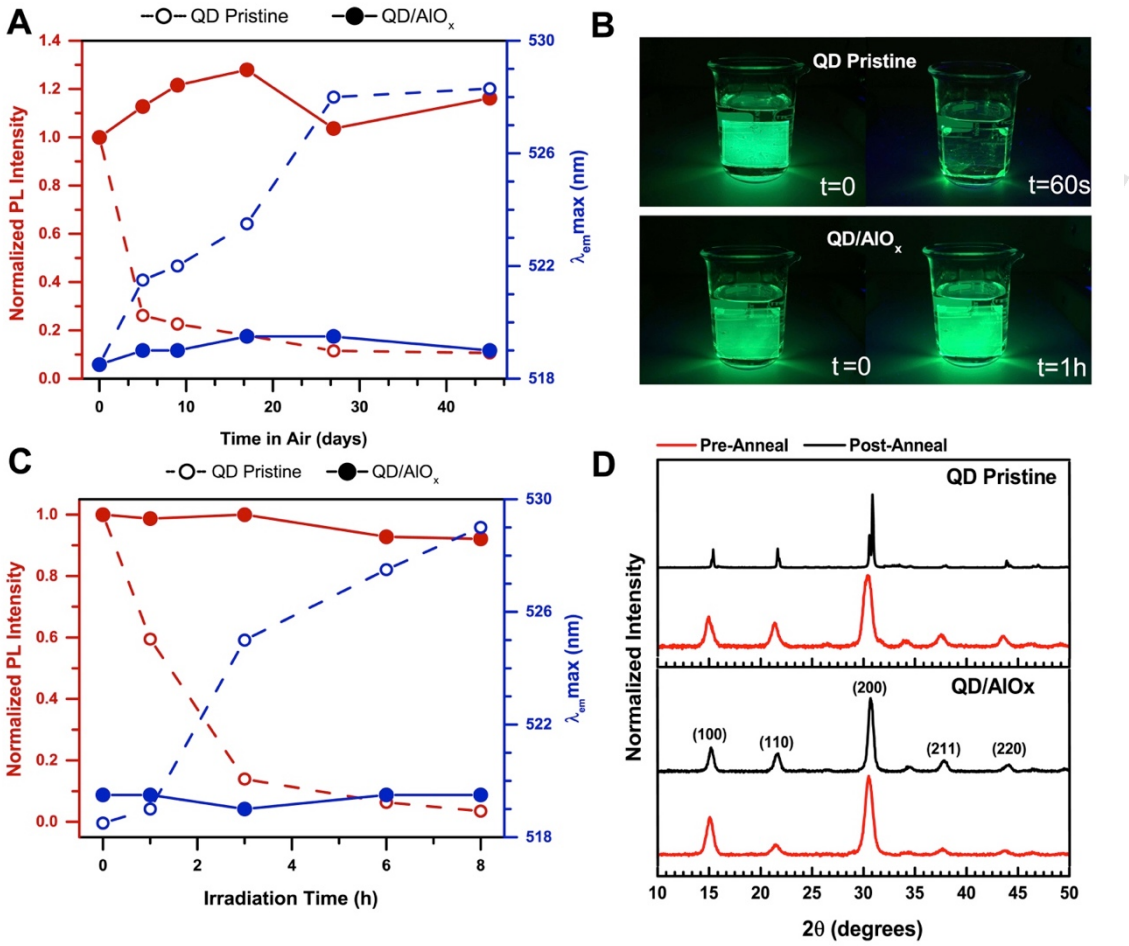

Figure 3: Stability studies on $CsPbBr_3$ QD/AlO_x nanocomposites obtained by performing 100 ALD cycles on 60 nm thick QD films. A) PL properties over 45 days of storage in ambient conditions. Red color shows changes in PL intensity and blue color shows changes in the PL peak position. B) Photographs taken under UV illumination (λ=365 nm) after 1 h of soaking in water. C) PL properties after 8 h photosoaking under solar spectrum irradiation at 10mW/cm^2. D) XRD spectra after annealing in air at 200 ºC.

The stability of the $CsPbBr_3$ QD/AlO_x nanocomposites was then tested in conditions which are expected to degrade the perovskite QDs: long-term storage in air, immersion in water, light irradiation, and annealing at relatively high temperatures (Figure 3).[9,37–39] Figure 3A shows a comparison of the PL properties between the pristine QDs and the nanocomposites as a function of the storage time in air. Over the course of 45 days, no apparent change was observed in the PL properties for the $CsPbBr_3$ QD/AlO_x nanocomposites. On the contrary, the pristine samples showed sharp PL quenching and a red-shift after only a few days of storage. Absorption measurements revealed similar behavior, indicative of rapid decomposition and sintering for untreated samples compared to long-term stability for the nanocomposites (Figure S13). Furthermore, the nanocomposites exhibited a striking improvement in stability when immersed in water as they were stable for at least 1 hour compared to immediate degradation observed for the pristine QDs (Figures 3B and S14, video in the Supporting Information). The crucial role of the overcoat layer as diffusion barrier to confer water stability to the nanocomposites was evidenced by testing QD films of the same thickness at varying ALD cycles (Figure S15). Interestingly, while only subtle structural differences were found when reducing t4 from 180 s to 20 s, the nanocomposites with lower purging time after the water pulse were less stable (Figure S16). A lower density of the alumina matrix and decreased conformity of the alumina layer on the QD surface might explain this observation.[17,31] The effect of the ALD treatment on the photostability of $CsPbBr_3$ QD films was studied. Photo-soaking experiments were conducted under simulated solar spectrum irradiation in air. Figure 3C evidences the dramatic PL intensity decay and energy red-shift of the pristine QDs that result from the combination of chemical and photo- degradation.[17,40] On the contrary, the nanocomposites are shown to be perfectly stable after 8 h of irradiation with no apparent PL quenching or energy shifting. However, when the irradiation power density was increased from 10 mW/cm^2 to 100 mW/cm^2, an irreversible PL intensity quenching of more than 50% after 8 h was observed, which stabilizes afterwards (Figure S17). Yet, absorption and XRD measurements showed no particular change after photosoaking, indicating that neither degradation nor sintering took place (Figure S18). Quenching was still observed in additional UV-filtered and air-free photosoaking experiments (Figure S19), which allows one to exclude the contribution of photochemical degradation of the ligands from the alumina band-gap (>3.4 eV) excitation and also

of UV-induced coarsening.[17,40] An alternative explanation for this quenching effect at higher irradiation densities is the photo-induced desorption of surface ligands and the subsequent formation of carrier trapping defects at high excitation intensities, as previously reported for chalcogenide QD films.[6,41,42] The effect of annealing on the $CsPbBr_3$ QD/AlO_x nanocomposites was investigated by heating the samples at 200ºC in air. Figure 3D shows the XRD spectra for the pristine QDs and the nanocomposites before and after annealing. Upon annealing, the pristine QD film shows additional peaks which are consistent with the presence of the thermodynamically stable orthorhombic phase (Figures S20-S21).[2],25,[43–48] On the contrary, there are no sintering and no additional XRD peaks in the nanocomposites (Figures S20-S21). All together, the stability tests point at the importance of combining the alumina infilling layer with the overcoat layer to build an effective protection scheme where the main function of the former is to prevent ion diffusion and thus sintering during annealing, while the latter is crucial to confer stability in water by acting as a diffusion barrier to oxygen and water.

Finally, the same ALD process was applied to obtain $CsPbI_3$ QD/AlO_x and $CsPb(I/Br)_3$ QD/AlO_x nanocomposites which possessed increased stability compared to the bare QD film counterparts as evidenced in Figures S22-S25. It should be noted that the $CsPbI_3$ QD/AlO_x, while more stable that the unprotected films, do not show exceptional stability, most likely as a result of the intrinsic instability of this particular composition.

In conclusion, inorganic perovskites QD thin films were stabilized by encapsulation in an alumina matrix deposited by ALD. The so-obtained $CsPbBr_3$ QD/AlO_x nanocomposites are highly uniform in morphology, homogeneous in composition and preserve over 50% of their PL. These nanocomposites are stable when exposed to air, to irradiation under solar spectrum irradiation at 10mW/cm^2, to thermal treatment at least up to 200 ºC in air, and to immersion in water. This general protection scheme is expected to impact the field tremendously by enabling fundamental studies, such as of exciton diffusion transport, which require the sample to be stable during the measurements, or of size-dependent phase transitions, where decoupling of size and sintering effects is necessary.[7],[49] Furthermore, this work will open the pathway towards new concepts for light absorbing architectures (i.e. based on Forster Transfer) and for more durable optoelectronic devices based on this exceptionally well performing new class of QDs.[2,36,50] Because this study highlights the importance of surface chemistry during the ALD process, future directions will focus on deepening the knowledge on the QD/TMA interaction and QD/AlO_x interface with the aim of driving the development of the ultimate ALD treatment so as to fully retain the optical properties of the pristine QDs and to improve their stability under simulated solar light.

Experimental Section

Experimental details are reported in the Supporting Information, which contain: details of material synthesis, characterization methods, TEM and SEM images, XRD patterns, PL, uv-vis absorption, XPS data, videos.

Acknowledgements

A.L acknowledges the H2020-Marie Curie Individual Fellowship with grant agreement number 701745 for financial support. R.B. thanks the Swiss SNF (AP Energy Grant, project number PYAPP2_166897/1). We thank Dr. Adam Shwartzberg for useful discussion on the ALD process, Daniele Laub for cross section TEM sample preparation, Gian Luca De Gregorio and Pascal Mieville for NMR and Mariateresa Scarongella for the QY measurements.

Keywords: perovskites • quantum dots • nanocomposites • atomic layer deposition • stability

[1] L. Protesescu, S. Yakunin, M. I. Bodnarchuk, F. Krieg, R. Caputo, C. H. Hendon, R. X. Yang, A. Walsh, M. V. Kovalenko, *Nano Lett.* **2015**, *15*, 3692–3696.

[2] A. Swarnkar, A. R. Marshall, E. M. Sanehira, B. D. Chernomordik, D. T. Moore, J. A. Christians, T. Chakrabarti, J. M. Luther, *Science.* **2016**, *354*, 92–95.

[3] B. R. Sutherland, E. H. Sargent, *Nat. Photonics* **2016**, *10*, 295–302.

[4] S. Yakunin, L. Protesescu, F. Krieg, M. I. Bodnarchuk, G. Nedelcu, M. Humer, G. De Luca, M. Fiebig, W. Heiss, M. V. Kovalenko, *Nat. Commun.* **2015**, *6*, 8056.

[5] S. A. Veldhuis, P. P. Boix, N. Yantara, M. Li, T. C. Sum, N. Mathews, S. G. Mhaisalkar, *Adv. Mater.* **2016**, *28*, 6804–6834.

[6] Y. Wang, X. Li, S. Sreejith, F. Cao, Z. Wang, M. C. Stuparu, H. Zeng, H. Sun, *Adv. Mater.* **2016**, *28,* 10637-10643.

[7] G. M. Akselrod, F. Prins, L. V. Poulikakos, E. M. Y. Lee, M. C. Weidman, A. J. Mork, A. P. Willard, V. Bulović, W. A. Tisdale, *Nano Lett.* **2014**, *14*, 3556–3562.

[8] J. Pan, S. P. Sarmah, B. Murali, I. Dursun, W. Peng, M. R. Parida, J. Liu, L. Sinatra, N. Alyami, C. Zhao, et al., *J. Phys. Chem. Lett.* **2015**, *6*, 5027–5033.

[9] M. Meyns, M. Perallvarez, A. Heuer-Jungemann, W. Hertog, M. Ibanez, R. Nafria, A. Genc, J. Arbiol, M. V. Kovalenko, J. Carreras, et al., *ACS Appl. Mater. Interfaces* **2016**, *8*, 19579–19586.

[10] F. Palazon, Q. A. Akkerman, M. Prato, L. Manna, *ACS Nano* **2016**, *10*, 1224–1230.

[11] G. Li, F. W. R. Rivarola, N. J. L. K. Davis, S. Bai, T. C. Jellicoe, F. De La Pe??a, S. Hou, C. Ducati, F. Gao, R. H. Friend, et al., *Adv. Mater.* **2016**, *28*, 3528–3534.

[12] H. C. Wang, S. Y. Lin, A. C. Tang, B. P. Singh, H. C. Tong, C. Y. Chen, Y. C. Lee, T. L. Tsai, R. S. Liu, *Angew. Chemie Int. Ed.* **2016**, 7924–7929.

[13] C. Sun, Y. Zhang, C. Ruan, C. Yin, X. Wang, Y. Wang, W. W. Yu, *Adv. Mater.* **2016**, 1–7.

[14] F. Bella, G. Griffini, J.-P. Correa-Baena, G. Saracco, M. Grätzel, A. Hagfeldt, S. Turri, C. Gerbaldi, *Science.* **2016**. *354,* 203-206.

[15] H. C. Weerasinghe, Y. Dkhissi, A. D. Scully, R. A. Caruso, Y.-B. Cheng, *Nano Energy*; **2015**, *18*. 118-125.

[16] A. Pourret, P. Guyot-Sionnest, J. W. Elam, *Adv. Mater.* **2009**, *21*, 232–235.

[17] Y. Liu, M. Gibbs, C. L. Perkins, J. Tolentino, M. H. Zarghami, J. Bustamante, M. Law, *Nano Lett.* **2011**, *11*, 5349–5355.

[18] B. Yin, B. Sadtler, M. Y. Berezin, E. Thimsen, *Chem. Commun.* **2016**, *52,* 11127-11130.

[19] E. Thimsen, S. V. Baryshev, A. B. F. Martinson, J. W. Elam, I. V. Veryovkin, M. J. Pellin, *Chem. Mater.* **2013**, *25*, 313–319.

[20] Y. Liu, J. Tolentino, M. Gibbs, R. Ihly, C. L. Perkins, Y. Liu, N. Crawford, J. C. Hemminger, M. Law, *Nano Lett.* **2013**, *13*, 130307111258007.

[21] K. Devloo-Casier, P. Geiregat, K. F. Ludwig, K. Van Stiphout, A. Vantomme, Z. Hens, C. Detavernier, J. Dendooven, *J. Phys. Chem. C* **2016**, *120*, 18039–18045.

[22] J. Ephraim, D. Lanigan, C. Staller, D. J. Milliron, E. Thimsen, *Chem. Mater.* **2016**, *28*, 5549–5553.

[23] K. Lambert, J. Dendooven, C. Detavernier, Z. Hens, *Chem. Mater.* **2011**, *23*, 126–128.

[24] H. M. So, H. Choi, H. C. Shim, S. M. Lee, S. Jeong, W. S. Chang, *Appl. Phys. Lett.* **2015**, *106*, 1–6.

[25] D. Valdesueiro, M. K. Prabhu, C. Guerra-Nunez, C. S. S. Sandeep, S. Kinge, L. D. A. Siebbeles, L. C. P. M. De Smet, G. M. H. Meesters, M. T. Kreutzer, A. J. Houtepen, et al., *J. Phys. Chem. C* **2016**, *120*, 4266–4275.

[26] F. Palazon, F. Di Stasio, S. Lauciello, R. Krahne, M. Prato, L. Manna, *J. Mater. Chem. C* **2016**, *4*, 9179–9182.

[27] Y. Yu, D. Zhang, C. Kisielowski, L. Dou, N. Kornienko, Y. Bekenstein, A. B. Wong, A. P. Alivisatos, P. Yang, *Nano Lett.* **2016**, acs.nanolett.6b03331.

[28] Y. Tong, E. Bladt, M. F. Aygüler, A. Manzi, K. Z. Milowska, V. A. Hintermayr, P. Docampo, S. Bals, A. S. Urban, L. Polavarapu, et al., *Angew. Chemie Int. Ed.* **2016**, *55*, 13887–13892.

[29] J. A. Sichert, Y. Tong, N. Mutz, M. Vollmer, S. Fischer, K. Z. Milowska, R. Garcia Cortadella, B. Nickel, C. Cardenas-Daw, J. K. Stolarczyk, et al., *Nano Lett.* **2015**, *15*, 6521–6527.

[30] J. De Roo, M. Ibáñez, P. Geiregat, G. Nedelcu, W. Walravens, J. Maes, J. C. Martins, I. Van Driessche, M. V. Kovalenko, Z. Hens, *ACS Nano* **2016**, *10*, 2071–2081.

[31] M. D. Groner, F. H. Fabreguette, J. W. Elam, S. M. George, *Chem. Mater.* **2004**, 639–645.

[32] I. Moreels, B. Fritzinger, J. C. Martins, Z. Hens, *JACS,* **2008,** *130*, 15081.

[33] I. Moreels, Y. Justo, B. De Geyter, K. Haustraete, J. C. Martins, Z. Hens, *ACS Nano.* **2011**, *5* (3). 2004.

[34] A. Gharachorlou, M. D. Detwiler, X. K. Gu, L. Mayr, B. Klötzer, J. Greeley, R. G. Reifenberger, W. N. Delgass, F. H. Ribeiro, D. Y. Zemlyanov, *ACS Appl. Mater. Interfaces* **2015**, *7*, 16428–16439.

[35] D. J. Weinberg, C. He, E. A. Weiss, *J. Am. Chem. Soc.* **2016**, *138*, 2319–2326.

[36] A. F. Palmstrom, P. K. Santra, S. F. Bent, *Nanoscale* **2015**, *7*, 12266–83.

[37] X. Zhao, N.-G. Park, *Photonics* **2015**, *2*, 1139–1151.

[38] H. Huang, B. Chen, Z. Wang, T. F. Hung, A. Susha, H. Zhong, A. Rogach, C. Sci, H. Huang, B. Chen, et al., *Chem. Sci.* **2013**, *0*, 1–3.

[39] J. M. Frost, K. T. Butler, F. Brivio, C. H. Hendon, M. Van Schilfgaarde, A. Walsh, *Nano Lett.* **2014**, *14*, 2584–2590.

[40] J. Chen, D. Liu, M. J. Al-Marri, L. Nuuttila, H. Lehtivuori, K. Zheng, *Sci. China Mater.* **2016**, *59*, 719–727.

[41] Y. Park, M. J. Felipe, R. C. Advincula, *ACS Appl. Mater. Interfaces* **2011**, *3*, 4363–4369.

[42] S. T. Malak, J. Jung, Y. J. Yoon, M. J. Smith, C. H. Lin, Z. Lin, V. V. Tsukruk, *Adv. Opt. Mater.* **2016**, 608–619.

[43] M. A. Van Huis, L. T. Kunneman, K. Overgaag, Q. Xu, G. Pandraud, H. W. Zandbergen, D. Vanmaekelbergh, *Nano Lett.* **2008**, *8*, 3959–3963.

[44] R. Ihly, J. Tolentino, Y. Liu, M. Gibbs, M. Law, *ACS Nano* **2011**, *5*, 8175–8186.

[45] R. C. Keitel, M. C. Weidman, W. A. Tisdale, *J. Phys. Chem. C.* **2016**, *120*(36), 20341-20349.

[46] R. E. Beal, D. J. Slotcavage, T. Leijtens, A. R. Bowring, R. A. Belisle, W. H. Nguyen, G. F. Burkhard, E. T. Hoke, M. D. McGehee, *J. Phys. Chem. Lett.* **2016**, 746–751.

[47] A. Pisoni, J. Jaćimović, O. S. Barišić, M. Spina, R. Gaál, L. Forró, E. Horváth, *J. Phys. Chem. Lett.* **2014**, *5*, 2488–2492.

[48] M. Koolyk, D. Amgar, S. Aharon, L. Etgar, *Nanoscale* **2016**, *8*, 6403–9.

[49] M. Liu, R. Y. Wang, *Sci. Rep.* **2015**, *5*, 16353.

[50] M. Kot, C. Das, Z. Wang, K. Henkel, Z. Rouissi, K. Wojciechowski, H. J. Snaith, D. Schmeisser, *ChemSusChem* **2016**, 1–7.